Editors' Suggestion

Anomalous transport in the Aubry-André-Harper model in isolated and open systems

Archak Purkayastha,[1] Sambuddha Sanyal,[2] Abhishek Dhar,[1] and Manas Kulkarni[1]
[1]*International Centre for Theoretical Sciences, Tata Institute of Fundamental Research, Bangalore 560089, India*
[2]*Department of Chemistry, Columbia University, 3000 Broadway, New York, New York 10027, USA*

(Received 24 February 2017; revised manuscript received 11 April 2018; published 24 May 2018)

We study the high-temperature transport behavior of the Aubry-André-Harper (AAH) model, both in an isolated thermodynamic limit and in an open system. At the critical point of the AAH model, we find hints of superdiffusive behavior from the scaling of spread of an initially localized wave packet. On the other hand, when connected to two baths with different chemical potentials at the two ends, we find that the critical point shows clear subdiffusive scaling of current with system size. We provide an explanation for this by showing that the current scaling with system size is entirely governed by the behavior of the single-particle eigenfunctions at the boundary sites where the baths are attached. We also look at the particle density profile in the nonequilibrium steady state of the open system when the two baths are at different chemical potentials. We find that the particle density profile has distinctly different behavior in the delocalized, critical, and localized phases of the AAH model.

DOI: 10.1103/PhysRevB.97.174206

I. INTRODUCTION

The absence of diffusion in noninteracting systems due to the presence of disorder is referred to as Anderson localization, which has been theoretically studied and experimentally observed in a wide class of systems, e.g., for electrons, photons, cold atoms, and sound waves [1–3]. The effect of localization is strongest in one dimension where it is known that a small amount of disorder localizes all states. If an interaction is switched on in such a localized system, a transition from the many-body localized (MBL) phase to delocalized phase can occur. The physics of the system close to the transition is not well understood and has received a lot of attention lately. One of the most interesting results of recent investigations is that close to the transition, one has Griffiths effects, leading to slow dynamics and subdiffusive transport [4–7].

An interesting class of models emerges when "true" disorder is replaced by a quasiperiodic potential. A paradigmatic example of such a system is the so-called Aubry-André-Harper (AAH) model [8,9]. This is a one-dimensional lattice model of noninteracting particles (bosons or fermions) in an incommensurate potential. For this system, one finds a remarkable transition from all energy eigenstates being localized to all states being extended as one decreases the strength of the potential. This transition is mediated by a critical point [8]. Unlike the MBL transition, this transition occurs in the absence of interactions. Also, Griffiths physics is not expected at this critical point because the potential is spatially correlated. Early studies found interesting features at the critical point, such as fractal patterns in the spectrum and the eigenstates [10–12]. It has also been extensively studied in the mathematical literature [13,14]. The AAH model and its various generalizations have received a lot of interest recently, both theoretically [15–36] and experimentally [37–43].

Although studies of wave-packet spreading in a closed system have shown hints of anomalous diffusion (as opposed to normal diffusion) behavior at the critical point [44–47], the exact nature of transport at the critical point has remained an open question. In the context of MBL, it has become most relevant because recent experiments investigating MBL physics are based on the AAH model with interactions, rather than a "truly" disordered system [37–40,42]. There has also been a lot of recent interest in disordered interacting systems connected to baths [38,48–57]. However, there have been only few studies on the open AAH system [23,30]. In particular, results on the nonlinear response of the system to external thermal or chemical potential biases are still lacking.

In this paper, we study the transport properties of the AAH model both in the isolated thermodynamic limit and in an open system. In the isolated thermodynamic limit we look at the spread of an initially localized wave packet and the conductivity calculated by the Green-Kubo formalism via numerical exact diagonalization. At the critical point, the integrated current autocorrelation appearing in the Green-Kubo conductivity seems to saturate to a constant value but with large fluctuations. Correspondingly, we find that the second moment for the spread of the wave packet goes as $\sim t$, and correctly gives a constant value in the Green-Kubo computation. However, we find that the tails of the wave packet spread superdiffusively. As a result, at very long times, the moments show a crossover from diffusive to superdiffusive behavior. This crossover occurs at shorter times for higher moments. A careful quantitative investigation shows that the time scales required to observe this crossover in the second moment are beyond our current computational power. This explains the normal-diffusive-like behavior of Green-Kubo conductivity and suggests that eventually, at extremely long times, the integrated current autocorrelation will diverge.

Next, we study the open system by connecting to two baths at the two ends. The baths are modeled by quadratic Hamiltonians with infinite degrees of freedom. We calculate the nonequilibrium steady state (NESS) current and particle density profile numerically exactly via the nonequilibrium Green's function (NEGF) approach. At the critical point, we find clear subdiffusive scaling of current with system

size, which is in sharp contrast to the properties of the isolated thermodynamic system discussed above. We provide an explanation for this by showing that the current scaling with system size is entirely governed by the behavior of the single-particle eigenfunctions at the boundary sites where the baths are attached. We further show that the NESS particle spatial density profile provides a real-space experimentally measurable probe of the localized, critical, and delocalized phases.

In Sec. II, we introduce the model, in Sec. III, we discuss the formalism and the results for transport behavior of the isolated system in the thermodynamic limit, in Sec. IV, we discuss the formalism and the results for the open system NESS, and in Sec. V, we give the conclusions.

II. MODEL

The AAH model is given by the Hamiltonian

$$\mathcal{H}_S = \sum_{r=1}^{N-1} (\hat{a}_r^\dagger \hat{a}_{r+1} + \text{H.c.}) + \sum_{r=1}^{N} 2\lambda \cos(2\pi b r + \phi) \hat{a}_r^\dagger \hat{a}_r, \quad (1)$$

where b is an irrational number, ϕ is an arbitrary phase, and $\hat{a}_r$ correspond to fermionic (bosonic) annihilation operators defined respectively on the rth lattice point of the system of N sites. The hopping parameter has been set to 1, and this is taken as the energy scale. When $\lambda < 1$, all the energy eigenstates of this model are delocalized, and when $\lambda > 1$, all the energy eigenstates are localized. $\lambda = 1$ is the critical point. This holds true for any choice of irrational number b and phase ϕ. The most popular choice for b is the golden mean $(\sqrt{5}-1)/2$. However, in experiments and numerics all numbers are essentially rational in a strict mathematical sense. The way around is given by the fact that for a system of finite size N, if b is taken as a rational number p/q with $q > N$, b remains "effectively irrational" and all the observed physics of AAH model is retained. In recent experiments [37–39], the physics of the AAH model has been explored by superimposing a 532-nm optical lattice with a 738-nm one, making $b = 532/738$. For $q < N$, the system becomes delocalized. Even though the choice of b is irrelevant for various interesting universal features of the AAH model, the exact nature of the plots depends on b. In this work, we have considered the following choices of b: golden mean $(\sqrt{5}-1)/2$, silver mean $\sqrt{2}-1$, and the rational number 532/738 used in the experiments in Refs. [37–39]. Further, we perform an average over the phase ϕ by numerically exactly integrating the final results between 0 and 2π and dividing by 2π.

III. TRANSPORT IN THE ISOLATED SYSTEM IN THE THERMODYNAMIC LIMIT

A. Formalism

We first look at the transport properties of the isolated system in the thermodynamic limit. For this we directly calculate the particle conductivity of the system using the Green-Kubo formula. For this, we define

$$\mathcal{G}(t) = \int_0^\beta d\lambda \sum_{p,q=1}^{N-1} \langle \hat{I}_p(-i\lambda) \hat{I}_q(t) \rangle / N, \quad (2)$$

where $\hat{I}_p = i(\hat{a}_p^\dagger \hat{a}_{p+1} - \hat{a}_{p+1}^\dagger \hat{a}_p)$, and $\langle \cdots \rangle = \text{Tr}\,(e^{-\beta(\mathcal{H}_S - \mu \mathcal{N}_S)}/Z \cdots)$. $\mathcal{N}_S = \sum_r \hat{a}_r^\dagger \hat{a}_r$ is the total number of particles in the system, and $Z = \text{Tr}(e^{-\beta(\mathcal{H}_S - \mu \mathcal{N}_S)})$. The conductivity by the Green-Kubo formalism is given by

$$\sigma_{\text{GK}} = \lim_{\tau \to \infty} \lim_{N \to \infty} D_N(\tau), \quad (3)$$

where

$$D_N(\tau) = \int_0^\tau \mathcal{G}(t) dt. \quad (4)$$

The order of limits in the Green-Kubo conductivity formula is important and cannot be interchanged, and the formula is strictly valid only for an infinite system size. But in numerics, one will always have a finite size. To go about numerically calculating the Green-Kubo conductivity, one has to look at the behavior $D_N(\tau)$ for a given system size, for times before the finite-size effects become substantial.

One can show that the Green-Kubo formula can be related to the spread of correlations. We start with the mixing assumption, expected to be valid in the thermodynamic limit. This says that, given two arbitrary operators Q_1 and Q_2, $\lim_{t\to\infty} \langle Q_1(t) Q_2(0) \rangle = \lim_{t\to\infty} \langle Q_1(t) \rangle \langle Q_2 \rangle$. Under this assumption, and time-translation and time-reversal symmetries, the Green-Kubo formula can be simplified to the form

$$\sigma_{\text{GK}} = \beta \lim_{\tau \to \infty} \lim_{N \to \infty} \int_0^\tau dt \sum_{p,q=1}^{N-1} \text{Re}(\langle \hat{I}_p(t) \hat{I}_q(0) \rangle)/N. \quad (5)$$

Starting from the continuity equation $\frac{d\hat{n}_p}{dt} = \hat{I}_p - \hat{I}_{p-1}$, where $\hat{n}_p = \hat{a}_p^\dagger \hat{a}_p$, it can be shown for the infinite-size system that

$$\frac{d}{d\tau} \sum_{x=-\infty}^{\infty} x^2 \langle \hat{n}_0(0) \hat{n}_x(\tau) \rangle = 2 \int_0^\tau dt \sum_{x=-\infty}^{\infty} \langle \hat{I}_0(0) \hat{I}_x(t) \rangle, \quad (6)$$

where we have used time-translation invariance as well as the space-translation invariance. The space-translation invariance is not present for our particular model in Eq. (1), but this is restored for quantities averaged over ϕ. Now, using translation invariance, it follows from Eqs. (5) and (6) that

$$\sigma_{\text{GK}} = \lim_{\tau \to \infty} \frac{\beta}{2} \frac{d}{d\tau} \text{Re} \left(\sum_{x=-\infty}^{\infty} x^2 \langle \hat{n}_0(0) \hat{n}_x(\tau) \rangle \right). \quad (7)$$

Note that here the $N \to \infty$ limit has already been taken before while using Eq. (6). For normal diffusive transport,

$$m_2^{nn}(\tau) = \text{Re} \left(\sum_{x=-\infty}^{\infty} x^2 \langle \hat{n}_0(0) \hat{n}_x(\tau) \rangle \right) = 2D\tau, \quad (8)$$

for large τ. Thus, the Green-Kubo conductivity for normal diffusive transport is given by

$$\sigma_{\text{GK}} = \lim_{\tau \to \infty} \lim_{N \to \infty} D_N(\tau) = \beta D. \quad (9)$$

Hence, for normal diffusive transport, we expect that, for large enough N, $D_N(\tau)$ will converge to this value as τ increases, before finite-size effects become substantial.

In general, $m_2^{nn}(t) \sim t^{2\tilde{\beta}}$. As seen above, $\tilde{\beta} = 0.5$, for normal diffusive transport. For ballistic transport, $\tilde{\beta} = 1$. If $0.5 < \tilde{\beta} < 1$, transport is superdiffusive. For both superdiffusive and

ballistic transports, as seen from Eqs. (7) and (8), the $\sigma_{\rm GK}$ diverges. If $0 < \tilde{\beta} < 0.5$, the transport is subdiffusive, while for a localized system, $\tilde{\beta} = 0$. In both these cases, $\sigma_{\rm GK}$ is zero. All cases other than the normal diffusive transport are broadly classified as anomalous transport.

This brings us to the study of $\langle \hat{n}_0(0)\hat{n}_x(\tau)\rangle$. In a very recent paper [16], the spread of a similar quantity was studied to classify transport behavior for the AAH model with interactions. Since our system is noninteracting, $\langle \hat{n}_x(t)\hat{n}_0(0)\rangle$ can be written down in terms of the single-particle eigenfunctions. We shift the origin to the site $N/2$ and define $x = r - N/2$. We have $\hat{a}_\ell(t) = \sum_{p=1}^{N} G(\ell,t|p,0)\hat{a}_p(0)$, where $G(\ell,t|p,0)$ is the single-particle Green's function for the closed system. Let $\Phi_{\alpha,\ell}$ be the ℓth component of the single-particle eigenvector corresponding to the single-particle energy eigenvalue ϵ_α. Thus, $\hat{a}_\ell = \sum_{\alpha=1}^{N} \Phi_{\alpha,\ell}\tilde{\hat{a}}_\alpha$, where $\tilde{\hat{a}}_\alpha$ are the annihilation operators in the eigenbasis. Here, α is the eigenstate index and ℓ is the site index. Then, $G(\ell,t|p,0) = \sum_{\alpha=1}^{N} e^{-i\epsilon_\alpha t}\Phi_{\alpha,\ell}\Phi_{\alpha,p}$. In terms of these, we have

$$\begin{aligned} C(x,t) =& \langle \hat{n}_x(t)\hat{n}_0(0)\rangle - \langle \hat{n}_x\rangle\langle \hat{n}_0\rangle \\ =& \Bigg[\sum_{\ell,p=1}^{N} G^*(x+N/2,t|\ell,0)G(x+N/2,t|p,0) \\ & \times \langle \hat{a}_\ell^\dagger(0)\hat{a}_{N/2}(0)\rangle\langle \hat{a}_p(0)\hat{a}_{N/2}^\dagger(0)\rangle\Bigg] \\ =& \sum_{\alpha,\nu=1}^{N}\big[\Phi_{\alpha,x+N/2}\Phi_{\nu,x+N/2}\Phi_{\alpha,N/2}\Phi_{\nu,N/2} \\ & \times e^{i(\epsilon_\alpha-\epsilon_\nu)t} n_F(\epsilon_\alpha)[1-n_F(\epsilon_\nu)]\big], \end{aligned} \tag{10}$$

where $n_F(\omega) = [e^{\beta(\omega-\mu)}+1]^{-1}$ is the Fermi distribution function.

Another related quantity that has been studied previously [44–47] for the AAH model is the spread of a wave packet. Let the wave packet $\psi_r(t)$ be initially localized at the site $N/2$ of the lattice. It evolves according to the Schrödinger equation

$$i\,\partial\psi_r/\partial t = \psi_{r+1}(t) + \psi_{r-1}(t) + 2\lambda\cos(2\pi br + \phi)\psi_r(t). \tag{11}$$

We look at the probability $P(x,t) = |\psi_x(t)|^2$, and its moments

$$m_{2p}(t) = \sum_{x=-N/2}^{N/2-1} (x - \langle x\rangle)^{2p} P(x,t), \tag{12}$$

where $\langle x\rangle = \sum_{x=-N/2}^{N/2-1} x\,P(x,t)$ is the mean. In terms of single-particle wave functions, $P(x,t)$ is given by

$$\begin{aligned} P(x,t) &= |G(x+N/2,t|N/2,0)|^2 \\ &= \sum_{\alpha,\nu=1}^{N}\Phi_{\alpha,x+N/2}\Phi_{\nu,x+N/2}\Phi_{\alpha,N/2}\Phi_{\nu,N/2}e^{i(\epsilon_\alpha-\epsilon_\nu)t}. \end{aligned} \tag{13}$$

This is different from $C(x,t)$ [see Eq. (10)] by only the factor $n_F(\epsilon_\alpha)(1-n_F(\epsilon_\nu))$ inside the summation. At high temperatures, $n_F(\omega) \sim 1/2$. Thus, at high temperatures,

$$\beta \to 0, \quad C(x,t) \to \frac{P(x,t)}{4}. \tag{14}$$

We are interested in the high-temperature transport. So the scaling properties of $C(x,t)$ and $P(x,t)$, and hence of $m_2^{nn}(t)$ and $m_2(t)$, will be the same.

For normal diffusive spreading, $P(x,t)$ has a Gaussian form, $P(x,t) = e^{-\frac{x^2}{16Dt}}/\sqrt{16\pi Dt}$, with this D the same as defined in Eq. (8). In general, if $P(x,t)$ [and thereby $C(x,t)$] scales as

$$P(x,t) \sim (1/t^{\tilde{\beta}})f(x/t^{\tilde{\beta}}), \tag{15}$$

then $[m_{2n}(t)]^{1/n} \sim t^{2\tilde{\beta}}$. The connection to different regimes of transport as discussed before is immediate. However, there may be cases where $\tilde{\beta} = 0.5$, but $P(x,t)$ is not Gaussian. Such "non-Gaussian but diffusive" transport has been reported in many classical systems [58–65]. This is also considered as anomalous transport. Further, there may even be cases where $P(x,t)$ does not follow a particular scaling form. As shown in Eq. (7), even then, the conductivity of the system depends only the time scaling of the second moment, and the classification of transport based on that is possible.

B. Results

With the above understanding, we numerically investigate the transport behavior of the AAH model in the isolated thermodynamic limit via exact diagonalization. All our results are given up to times before finite-size effects become substantial. We are primarily interested in the transport properties of the AAH model at the critical point ($\lambda = 1$). Figure 1 shows a plot of $D_N(\tau)$ with τ for different system sizes, at the critical point for $b = \sqrt{2}-1$. We see that with increasing N, $D_N(\tau)$ converges to a curve which initially increases and then shows large fluctuations about a constant mean value. Consistently, $m_2^{nn}(t) \sim 0.288t$, and the mean value is precisely given by βD [see Eqs. (8) and (9)]. This seems to suggest that $\sigma_{\rm GK}$ is finite in the thermodynamic limit, which is akin to a normal "diffusive" system. However, the fluctuations do not decrease on averaging over ϕ, and may indicate deviation from normal diffusive transport.

To investigate more closely the nature of transport at the critical point, we now look at the scaling of $P(x,t)$. This is shown in Fig. 2 for various choices of b. It is clear that although $m_2(t) \sim t$, $P(x,t)$ is non-Gaussian, and does not obey a single scaling form. The bulk of $P(x,t)$ has the scaling form of Eq. (15), with $\tilde{\beta} = 0.5$ for all choices of b. However, the tails of $P(x,t)$ do not collapse under the same scaling. This deviation from bulk scaling is most clearly seen for $b = \sqrt{2}-1$. To collapse the tails of $P(x,t)$, one needs a superdiffusive scaling. Thus we find

$$P(x,t) = \begin{cases} (1/\sqrt{t})f_1(x/\sqrt{t}), & \forall |x| \leqslant z_0\sqrt{t}, \\ (1/t^{\tilde{\beta}_2})f_2(x/t^{\tilde{\beta}_2}),\ \tilde{\beta}_2 > 0.5, & \forall |x| > z_0\sqrt{t}, \end{cases} \tag{16}$$

where z_0 and $\tilde{\beta}_2$ depend on the choice of b. Note that z_0 is independent of time. The superdiffusive scaling exponent $\tilde{\beta}_2$ is nonuniversal and depends on the choice of

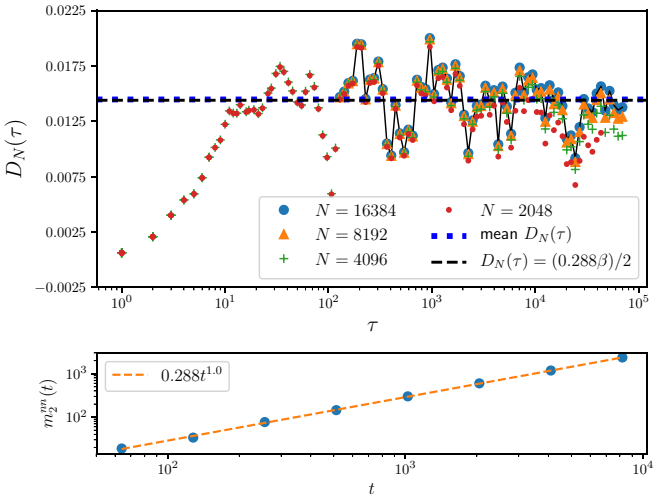

FIG. 1. Isolated thermodynamic limit: The top panel shows the plot of $D_N(\tau)$ as a function of τ at the critical point $\lambda = 1$ for different system sizes. $D_N(\tau)$ initially increases with τ and then shows large fluctuations about a constant mean value. This mean value is quite precisely given by the analytical high-temperature approximation result $D_N(\tau) \simeq \beta D$. D is obtained by time scaling of m_2^{nn} [Eq. (8)] shown in the bottom panel. $D = 0.288/2$. For $N = 8192$ and 16 384, only the large time results have been calculated. The black continuous line is a guide to the eye joining data points for $N = 16\,384$. The mean $D_N(\tau)$ is calculated from the data points for $N = 16\,384$. Parameters: $\beta = 0.1$, $\mu = 1$, $b = \sqrt{2} - 1$.

b. For $b = (\sqrt{5} - 1)/2$ and for $b = 532/738$, $\tilde{\beta}_2 \sim 0.55$, for $b = \sqrt{2} - 1$, $\tilde{\beta}_2 \sim 0.62$.

Note that for $b = (\sqrt{5} - 1)/2$ and $b = 532/738$, from Fig. 2(b) it may seem that the superdiffusive scaling of $P(x,t)$ holds everywhere. This is because the superdiffusive exponent 0.55 is quite close to 0.5. However, a closer inspection reveals that this is not the case, and the bulk indeed has a diffusivelike scaling. This is clear from the fact that in all cases, $m_2(t)$ in Fig. 2(c) shows diffusive behavior, $m_2(t) \sim t$, and not superdiffusive behavior. Also note that, for $b = \sqrt{2} - 1$, $m_2(t) \sim 1.15t \simeq 4m_2^{nn}(t)$, consistent with Eq. (14).

Now, let us see if the behavior of the tails of $P(x,t)$ can affect the scaling of the moments at extremely long times. To check this, we write $m_{2p}(t)$ as

$$\begin{aligned} m_{2p}(t) &= 2\sum_{x=0}^{x\leqslant z_0\sqrt{t}} x^{2p}P(x,t) + 2\sum_{x>z_0\sqrt{t}}^{\infty} x^{2p}P(x,t) \\ &\simeq 2\int_0^{z_0\sqrt{t}} x^{2p}P(x,t)dx + 2\int_{z_0\sqrt{t}}^{\infty} x^{2p}P(x,t)dx \\ &\equiv m_{2p}^{(1)}(t) + m_{2p}^{(2)}(t), \end{aligned} \tag{17}$$

where $m_{2p}^{(1)}(t)$ is the contribution to the moment from the diffusive part, while $m_{2p}^{(2)}(t)$ is the contribution to the moment from the tails. Here, we have used the fact that $\langle x \rangle = 0$, and $P(x,t)$ is an even function of x. Now, changing variables to

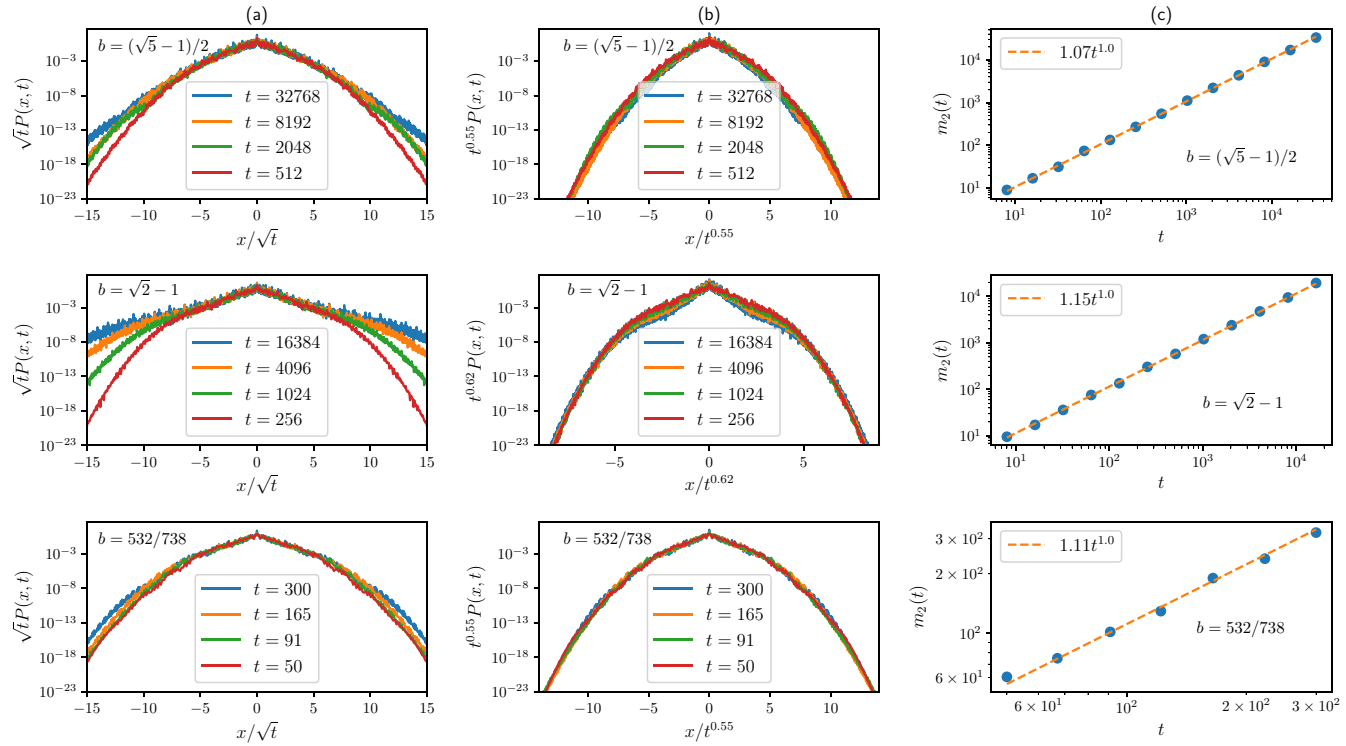

FIG. 2. Isolated thermodynamic limit: (a) The full distributions $P(x,t) = |\psi(x,t)|^2$, scaled assuming normal diffusive behavior. Here, $x = r - N/2$. $P(x,t)$ scales as $P(x,t) \simeq (1/\sqrt{t})f_1(x/\sqrt{t})$ over a considerable region in the bulk, but the scaling function $f_1(z)$ is clearly not Gaussian and also the tails do not collapse. (b) $P(x,t) = |\psi(x,t)|^2$ scaled to collapse the tails of the distribution. The tails show a superdiffusive scaling $P(x,t) \simeq (1/t^{\tilde{\beta}})f_2(x/t^{\tilde{\beta}})$ with $\tilde{\beta} > 0.5$. However, the value of $\tilde{\beta}$ depends on the choice of b. (c) The scaling of the second moment $m_2(t)$ of $P(x,t)$ with t for various values of b. $m_2(t) \sim t$. $N = 8192$ for $b = (\sqrt{5} - 1)/2$, $\sqrt{2} - 1$. $N = 700$ for $b = 532/738$.

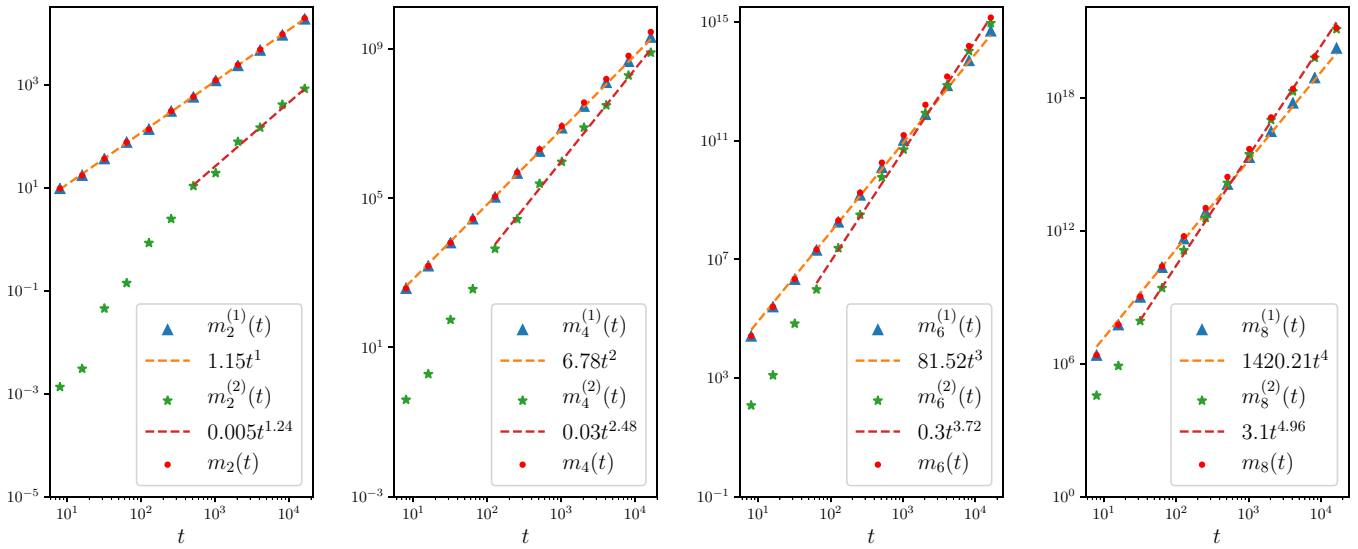

FIG. 3. Isolated thermodynamic limit: Plots of $m_{2p}^{(1)}(t)$, $m_{2p}^{(2)}(t)$, and $m_{2p}(t)$ [see Eq. (17)] with time for $b=\sqrt{2}-1$. $z_0=5$. The dashed lines are fits for $m_{2p}^{(1)}(t)$ and $m_{2p}^{(2)}(t)$. $m_{2p}^{(1)}(t)\sim t^p$, whereas $m_{2p}^{(2)}(t)\sim t^{0.62p}$ for large t, as expected from tail scaling of $P(x,t)$. The crossover of m_{2p} scaling from diffusive to superdiffusive is seen clearly for $m_8(t)$ and $m_6(t)$. From the scaling fits, we see that for $m_2(t)$ this crossover will occur for time $t\gg 10^{10}$. $N=8192$.

$z_1=x/\sqrt{t}$ and $z_2=x/t^{\tilde{\beta}_2}$, and using Eq. (16), we have

$$m_{2p}(t)\simeq 2t^p\int_0^{z_0} z_1^{2p} f_1(z_1)dz_1+2t^{2p\tilde{\beta}_2}\int_{z_0\sqrt{t}/t^{\tilde{\beta}_2}}^{\infty} z_2^{2p} f_2(z_2)dz_2$$
$$=2t^{2p\tilde{\beta}_2}\left[t^{p(1-2\tilde{\beta}_2)}A_p+F_p(z_0t^{0.5(1-2\tilde{\beta}_2)})\right], \quad (18)$$

where $A_p=\int_0^{z_0} z_1^{2p} f_1(z_1)dz_1$ and $F_p(\tau)=\int_\tau^\infty z_2^{2p} f_2(z_2)dz_2$. Note that A_p is independent of time while F_p is a function of time. So $m_{2p}^{(1)}(t)\sim t^p$, whereas $m_{2p}^{(2)}(t)\sim t^{2p\tilde{\beta}_2}$ only asymptotically. Since $\tilde{\beta}_2>0.5$, we have

$$m_{2p}(t)\sim 2t^{2p\tilde{\beta}_2}F_p(0), \quad t\to\infty. \quad (19)$$

Thus, the extremely long-time behavior of the moments should be superdiffusive. Hence, there will be a crossover in the time scaling of the moments from diffusive to superdiffusive. The approach to superdiffusive scaling is faster for higher moments. Let us check this quantitatively for $b=\sqrt{2}-1$, which is the case where $\tilde{\beta}_2\sim 0.62$ differs most significantly from the value 0.5. The value of z_0 can be read off from Fig. 2 as $z_0\sim 6$. Figure 3 shows the plots of $m_{2p}(t)$, $m_{2p}^{(1)}(t)$, $m_{2p}^{(2)}(t)$ for $p=1,2,3,4$. The first feature to note is that the approach to the form $m_{2p}^{(2)}(t)\sim t^{2p\tilde{\beta}_2}$ is faster for higher moments. Second, as expected, the crossover to superdiffusive scaling of $m_{2p}(t)$ also occurs faster for higher moments. For $m_8(t)$ and $m_6(t)$, this crossover is clearly seen from our data. On the other hand, for $m_4(t)$ and $m_2(t)$, the crossover occurs later than times accessible in our numerics. From the scaling fits, it is possible to quantitatively extract the time scales at which the superdiffusive crossover will be seen in the $m_2(t)$ scaling. We find that the superdiffusive scaling of $m_2(t)$ will start showing for $t\gg t^*\sim 10^{10}$. To directly investigate such long-time behavior without having finite-size effects, one needs systems of size $N\gg (t^*)^{0.62}\sim 10^7$. An exact numerical analysis of such system sizes is definitely beyond our current computational power. This explains the normal-diffusive-like behavior of Green-Kubo conductivity up to times and system sizes within our numerical reach, and suggests that at even longer times, the superdiffusive behavior will show up.

Therefore, we find *hints of superdiffusive behavior at the critical point of the AAH model in the isolated thermodynamic limit* from the tail scaling of $P(x,t)$ and the time scaling of higher moments of $P(x,t)$. However, a direct numerical observation of this superdiffusive behavior from $m_2(t)$ scaling or from Green-Kubo conductivity is beyond our current numerical reach. Within our numerical reach, $m_2(t)$ scales

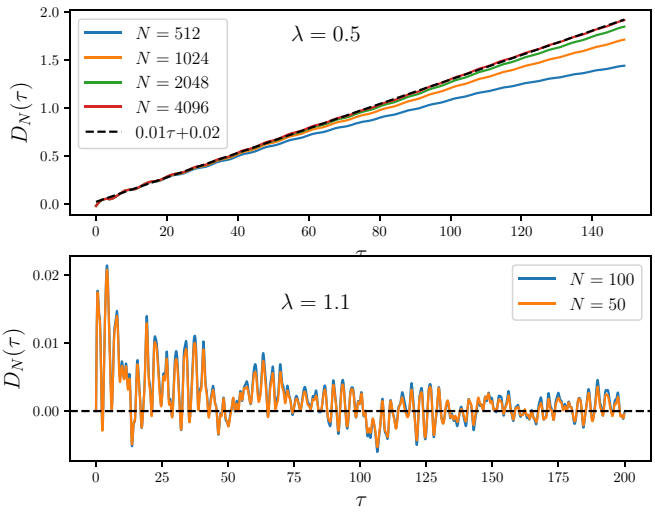

FIG. 4. Isolated thermodynamic limit: Plot showing $D_N(\tau)$ as a function of τ for delocalized (top panel) and localized (bottom panel) cases for different system sizes. For the delocalized case, $D_N(\tau)$ increases linearly with τ before finite-size effects come into play. For the localized case, $D_N(\tau)$ decays to zero and is independent of N for $N\gg$ localization length $=1/\log(\lambda)\simeq 10$. Parameters: $\beta=0.1$, $\mu=1$, $b=\sqrt{2}-1$.

diffusively, and Green-Kubo conductivity also shows normal-diffusive-like behavior.

Away from the critical point, the behavior is exactly as expected. Plots of $D_N(\tau)$ for delocalized and localized regimes are shown in Fig. 4 for $b = \sqrt{2} - 1$. In the delocalized regime ($\lambda < 1$), $D_N(\tau)$ increases linearly with τ before finite-size effects become significant. Finite-size effects start showing after times of $O(N)$. Thus, to numerically take the correct limit [in Eq. (3)] for a given system size N, one needs to look at $\tau \sim N$. This correctly gives the ballistic conductivity scaling with system size, $\sigma \sim N$. It is also trivial to check $m_2(t) \sim t^2$. In the localized regime ($\lambda < 1$), for system sizes much greater than the localization length [given by $1/\log(\lambda)$ [8]], the thermodynamic limit is reached and $D_N(\tau)$ becomes independent of N. We see $D_N(\tau)$ decays to zero as a function of τ for such cases, thus giving zero conductivity. Obviously, because all eigenstates are localized, $m_2(t) \sim t^0$ consistently.

We will show below that, when the system is connected to baths, the transport behavior at the critical point of the AAH model completely changes.

IV. TRANSPORT IN THE OPEN SYSTEM

A. Formalism

Having investigated the transport properties of the isolated AAH model, we now look at transport properties of the open AAH model, i.e., when the AAH system is connected to baths. For this, we couple the system Hamiltonian $\mathcal{H}_S$ [Eq. (1)] bilinearly with two baths at two ends. The baths are modeled by noninteracting Hamiltonians with infinite degrees of freedom. The full Hamiltonian of the system+bath reads as $\mathcal{H} = \mathcal{H}_S + \mathcal{H}_B + \mathcal{H}_{SB}$, where

$$\begin{aligned}\hat{\mathcal{H}}_B &= \hat{\mathcal{H}}_B^{(1)} + \hat{\mathcal{H}}_B^{(N)},\\ \hat{\mathcal{H}}_B^{(p)} &= \sum_s \Omega_{ps}\hat{B}_{ps}^\dagger \hat{B}_{ps}, \quad p = 1, N,\\ \hat{\mathcal{H}}_{SB} &= \sum_s (\tilde{\kappa}_{ps}\hat{B}_{ps}^\dagger \hat{a}_p + \text{H.c.}).\end{aligned} \tag{20}$$

Here, $\hat{B}_{ps}$ is the annihilation operator of the sth mode of the bath attached to the pth site of the system. The baths are connected at the first and the Nth sites of the system. Here, we consider the case where all operators are fermionic. However, since we will be looking at high-temperature behavior, the all-operator bosonic case will give identical results. We assume that, initially, each of the two baths is at thermal equilibrium at its own temperature and chemical potential. In this paper, we present results for the case when the two baths are at the same temperature but have different chemical potentials, thereby having a voltage bias. So, we introduce the bath Fermi distributions,

$$n_F^{(p)}(\omega) = [e^{\beta(\omega-\mu_p)} + 1]^{-1}, \quad p = 1, N. \tag{21}$$

But, again, in the high-temperature regime, our results remain valid for the case of both thermal and chemical potential biases. Let us also introduce the bath spectral functions,

$$J_p(\omega) = 2\pi \sum_s |\tilde{\kappa}_{ps}|^2 \delta(\omega - \Omega_{ps}), \quad p = 1, N. \tag{22}$$

We assume the two bath spectral functions to be identical, $J_1(\omega) = J_N(\omega) = J(\omega)$.

We are interested in the nonequilibrium steady state (NESS) of this setup. The NESS properties of this setup can be exactly calculated via nonequilibrium Green's function (NEGF) formalism. The system Hamiltonian can be written as $\mathcal{H}_S = c^\dagger \mathbf{H}_S c$, with c being the column vector with the jth element $c_j = \hat{a}_j$ and $c^\dagger$ is the transpose conjugate. Let $\mathcal{G}(\omega) = \mathbf{M}^{-1}(\omega)$ be the NEGF of the setup. $\mathbf{M}(\omega)$ is given by the $N \times N$ matrix,

$$\mathbf{M}(\omega) = [\omega \mathbf{I} - \mathbf{H}_S - \Sigma^{(1)}(\omega) - \Sigma^{(N)}(\omega)], \tag{23}$$

where $\Sigma^{(1)}(\omega), \Sigma^{(N)}(\omega)$ are the bath self-energy matrices with the only nonzero elements given by

$$\Sigma_{pp}^{(p)}(\omega) = -\mathcal{P}\int \frac{d\omega' J(\omega')}{2\pi(\omega' - \omega)} - \frac{i}{2}J(\omega), \quad p = 1, N, \tag{24}$$

where $\mathcal{P}$ denotes the principal value. The NESS quantities of our interest will be the (particle) current I and the occupation of the rth site $\langle \hat{n}_r \rangle$. These are given by

$$\begin{aligned} I &= \int \frac{d\omega}{2\pi} T(\omega)\left[n_F^{(1)}(\omega) - n_F^{(N)}(\omega)\right],\\ T(\omega) &= \frac{J^2(\omega)}{|\det[\mathbf{M}(\omega)]|^2},\\ \langle \hat{n}_r \rangle &= \int \frac{d\omega}{2\pi}\left[|\mathcal{G}_{r1}(\omega)|^2 n_F^{(1)}(\omega) + |\mathcal{G}_{rN}(\omega)|^2 n_F^{(N)}(\omega)\right], \end{aligned} \tag{25}$$

where $T(\omega)$ is the transmission function. In the linear response regime, the expression for (particle) conductance G is given by

$$G = \beta \int \frac{d\omega}{2\pi} T(\omega) n_F(\omega)[1 - n_F(\omega)]. \tag{26}$$

Note that all information about the explicit model of the bath is now in $J(\omega)$. Different noninteracting baths correspond to different choices of $J(\omega)$. For concreteness, in the following, we choose

$$J(\omega) = \frac{2\gamma^2}{t_B}\sqrt{1 - \left(\frac{\omega}{2t_B}\right)^2}, \tag{27}$$

which can be explicitly derived if baths are modeled via semi-infinite tight-binding chains with a hopping parameter t_B and bilinearly connected to the system at one end via system-bath coupling γ [66]. If all operators were bosonic, only the Fermi distributions in Eq. (25) would be replaced by the corresponding Bose distribution.

The main characterization of transport in the open system is via the system-size scaling of current I. At high temperatures, the current I and the conductance G scale the same way. The conductivity in the thermodynamic limit as obtained from the open system approach is given by

$$\sigma_{\text{open}} = \lim_{N\to\infty} NG \simeq \lim_{N\to\infty} NI/(\mu_1 - \mu_2). \tag{28}$$

At very high temperatures,

$$I \simeq (\mu_1 - \mu_2)G \simeq (\mu_1 - \mu_2)(\beta/4)\int \frac{d\omega}{2\pi} T(\omega), \quad \forall\, \beta \to 0. \tag{29}$$

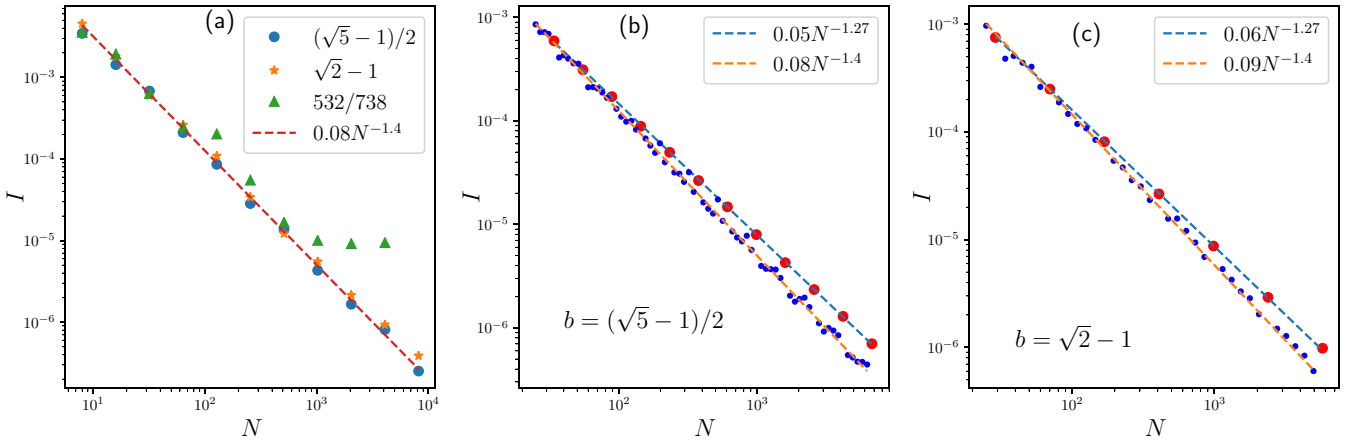

FIG. 5. Open system: (a) Scaling of current I with system size N for various values of b. $I \sim N^{-1.4\pm0.05}$. For $b = 532/738$, current scaling shows ballistic behavior, $I \sim N^0$ for $N \gg 738$, as expected. Here, the system sizes taken are powers of 2. (b) Scaling of current with system size for $b = (\sqrt{5}-1)/2$ with many closely taken points. This reveals that $I \sim N^{-1.27\pm0.01}$ for $N =$ Fibonacci numbers (red circles), whereas $I \sim N^{-1.4\pm0.05}$ for system sizes away from Fibonacci numbers. (c) Scaling of current with system size for $b = \sqrt{2}-1$ with many closely taken points. This reveals that $I \sim N^{-1.27\pm0.01}$ for $N =$ Pell numbers (red circles), whereas $I \sim N^{-1.4\pm0.05}$ for system sizes away from Pell numbers. Parameters : $\beta = 0.1$, $\mu_1 = 3$, $\mu_2 = -3$, $\gamma = 1$, $t_B = 3$.

For a diffusive system, conductivity is finite, so $I \sim N^{-1}$. For ballistic transport, the current is independent of system size, so $I \sim N^0$. If $I \sim N^{-\alpha}$, with $0 < \alpha < 1$, the transport is superdiffusive. In both superdiffusive and ballistic cases, σ_{open} diverges. If $I \sim N^{-\alpha}$, with $\alpha > 1$, the transport is subdiffusive, while for a localized system, $I \sim e^{-N}$, and in these cases, σ_{open} vanishes.

The fundamental difference between σ_{open} and σ_{GK} is the following. In calculating σ_{GK}, as given in Eq. (3), the thermodynamic limit $N \to \infty$ is taken before taking the $t \to \infty$ limit. As a consequence, the system can be considered really isolated and there is no effect of any bath. On the other hand, in calculating σ_{open}, the $t \to \infty$ limit is taken first so that the NESS is reached, and then the $N \to \infty$ limit is taken. A detailed and rigorous discussion regarding this is given in Ref. [67]. Physically, in the open system approach, there is the effect of a boundary between the system and the bath, while in the Green-Kubo approach, because of taking the thermodynamic limit first, there is no boundary. As we will see below, the occurrence of the boundary drastically changes the transport properties of the open AAH model at the critical point. We will also see that the NESS particle density profile has very different behavior in the three phases of the AAH model.

B. Results

1. Current scaling with system size

The current scaling with system size at the critical point for various choices of b is shown in Fig. 5(a). Here, system sizes were taken as powers of 2. It is immediately clear that the scaling is subdiffusive with $I \sim N^{-1.4\pm0.05}$. It is also interesting to note that for $b = 532/738$ the current becomes independent of N for $N \gtrsim 738$, which is the signature of the delocalized phase. This is consistent with our previous discussion that 532/738 remains "effectively irrational" only for $N \lesssim 738$.

In Figs. 5(b) and 5(c), we investigate the current scaling with system size more closely for the golden mean and silver mean cases. We see that for the golden (silver) mean, the current scaling with system size is different for system sizes equal to Fibonacci (Pell) numbers, where $I \sim N^{-1.27\pm0.01}$. Away from these special system sizes, the current scaling is approximately $I \sim N^{-1.4\pm0.05}$. An interesting observation follows from noting that any irrational number has an infinite continued fraction representation which, on truncation, gives a rational approximation of the irrational number. We conjecture that at special system sizes equal to the denominators of the rational approximations, the current deviates from the generic behavior and has a different scaling. These special system sizes are the Fibonacci (Pell) numbers for the golden (silver) mean.

Thus, we see that the *transport in the open critical AAH model is subdiffusive*. This is drastically different from what we found in the isolated thermodynamic limit, where we found hints of superdiffusive behavior. We now investigate the origin of the subdiffusive behavior. To do this, we first take the $t_B \to$ large limit, so that the system-bath coupling becomes weak and the bath spectral functions become almost constant [see Eq. (27)]. Note that in Fig. 5, the system-bath coupling was not weak. In the weak system-bath coupling limit, it is possible to express the steady state expressions, involving nonequilibrium Green's functions, directly in terms of the eigenstates and eigenvalues of the isolated system [68,69]. Using the formalism in Ref. [66], it can be shown [70] that for sufficiently small system-bath coupling, the conductance is given by

$$G \simeq \frac{\Gamma\beta}{4} W(1,N), \quad \beta \to \text{small}, \quad t_B \to \text{large},$$
$$W(p,q) = \sum_{\alpha=1}^{N} \frac{\Phi_{\alpha,p}^2 \Phi_{\alpha,q}^2}{\Phi_{\alpha,p}^2 + \Phi_{\alpha,q}^2}, \tag{30}$$

where $\Gamma = (2\gamma^2)/t_B$ and we have also taken the small β limit so that $n_F(\omega) \simeq 1/2$. Thus, the system-size scaling of G in

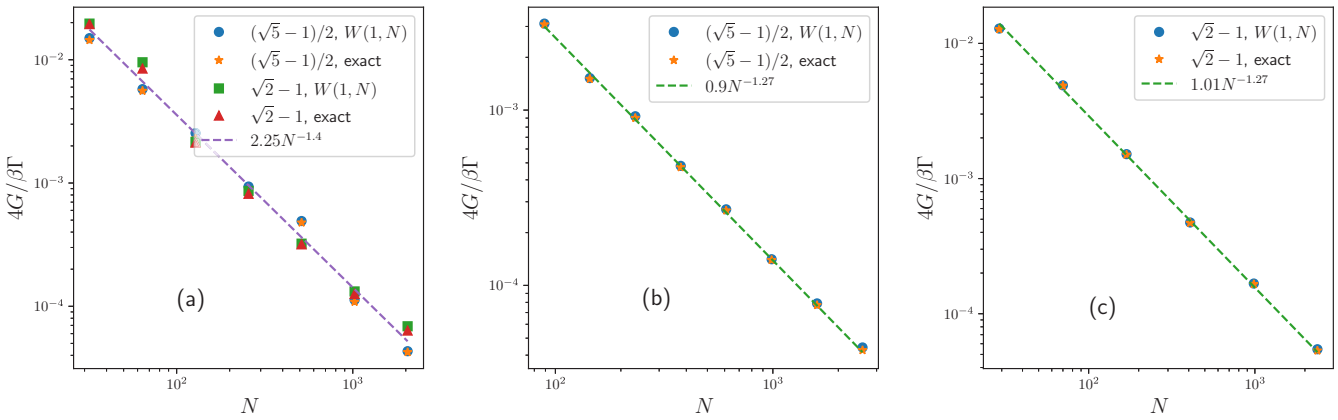

FIG. 6. Open system: (a) Scaling of conductance G with system size N for various values of b for weak system-bath coupling ($\gamma = 1$, $t_B = 200$) and very high temperature ($\beta = 0.01$). Exact numerical results are obtained via Eq. (26), and are compared with the approximate analytical result $W(1,N)$ [see Eq. (30)]. There is a nearly perfect overlap of exact results with $W(1,N)$, and $G \sim N^{-1.4\pm0.05}$. Here, the system sizes taken are powers of 2. (b), (c) The different scaling of G with system size equal to Fibonacci and Pell numbers for golden mean and silver mean cases, $G \sim N^{-1.27\pm0.01}$.

this limit is given by the system-size scaling of $W(1,N)$. Note that $W(1,N)$ only depends on the absolute values of the single-particle eigenvectors of the system at sites where the baths are attached, namely, the first and the last sites. If the system-size scaling of G in this limit is similar to that in Fig. 5, which is not guaranteed *a priori*, we will know that the subdiffusive scaling is because of the system-size scaling of $W(1,N)$.

The system-size scaling of conductance calculated in this limit ($\gamma = 1$, $t_B = 200$, $\beta = 0.01$) by exact numerical integration, Eq. (26), and by Eq. (30) is given in Fig. 6. There is a nearly perfect overlap of the two results. Note that an exact numerical calculation using Eq. (26) is more difficult in this regime, because of the nearly singular behavior of the integrand at the system eigenenergies. In Fig. 6(a), the scaling is shown for system sizes in powers of 2. The scaling is not as good as that seen in the strong system-bath coupling case, but it is approximately the same, $G \sim N^{-1.4\pm0.05}$. Figure 6(b) [Fig. 6(c)] shows the scaling for the golden (silver) mean case when the system sizes are equal to Fibonacci (Pell) numbers. Here, there is an almost perfect scaling of $G \sim N^{-1.27\pm0.01}$, as before. Thus, indeed, the subdiffusive scaling of current and conductance with system size is directly related to the subdiffusive scaling of $W(1,N)$ with system size.

Note that, for $\lambda < 1$, the single-particle eigenfunctions are completely delocalized, hence $\Phi^2_{\alpha,\ell} \sim N^{-1}$. Thus, $W(1,N) \sim N^0$, thereby consistently giving the ballistic scaling of current. On the other hand, for $\lambda > 1$, the single-particle eigenfunctions are exponentially localized at some system site, so, $\Phi^2_{\alpha,1} \sim \Phi^2_{\alpha,N} \sim e^{-N}$. Thus, $W(1,N) \sim e^{-N}$, thereby also consistently giving the exponential decay of current with system size in this regime. Thus, the system-size scaling of $W(1,N)$ correctly gives the system-size scaling of currents at all regimes of the AAH model. This also shows that the current scaling with system size is independent of the details of the baths, and also independent of the type of particles (bosonic or fermionic).

Hence, the transport behavior of the open AAH model is completely governed by the single-particle eigenfunctions at the boundaries where the baths are attached. In the isolated thermodynamic limit, there are no boundaries, and the transport behavior is governed by the bulk properties. Looking at Eqs. (7), (10), (13), and (30), we see that there is no reason *a priori* that the isolated thermodynamic limit transport characterized by the spread of a wave packet, and the open system transport characterized by current scaling with system size, need to be consistent with each other in general. It nonetheless turns out that in the delocalized and the localized cases, they can indeed be shown to be consistent. The underlying reason for this is that, for these cases, the eigenstates contributing to transport have similar behavior in the bulk and at the boundaries. But, at the critical point, the eigenstates contributing to transport have different behavior at the bulk and at the boundaries. To clearly see this, in Fig. 7 we check the system-size scaling of $W(N/4,3N/4)$ for all three phases and compare them with that of $W(1,N)$. Unlike $W(1,N)$, $W(N/4,3N/4)$ depends on the bulk behavior of eigenstates. We see that at the critical point, $W(N/4,3N/4)$ scales very differently from $W(1,N)$, i.e., $W(N/4,3N/4) \sim N^{-0.27\pm0.03}$ whereas $W(1,N) \sim N^{-1.4\pm0.05}$. Away from the critical point, $W(N/4,3N/4)$ and $W(1,N)$ have the same scaling with system size, i.e., they are independent of N for $\lambda < 1$ and decay exponentially with N for $\lambda > 1$. Thus, indeed, the eigenstates contributing to transport have different behavior in the bulk and at the boundaries only at the critical point. This leads to drastically different transport behavior in the isolated and in the open critical AAH model. We note that differences between the bulk and boundary behavior of the eigenstates have been previously observed in disordered systems and have been attributed to the multifractal nature of the eigenfunctions [1], but they have not been directly connected to transport properties.

2. NESS particle density profile

Next, we look at the spatial particle density profile, $\langle \hat{n}_r \rangle$ vs r, in NESS in each of the delocalized, critical, and localized regimes when the two baths are at widely different chemical potentials. We find that the NESS spatial particle density profile (which is related to the local chemical potential) behaves very differently in the three regimes (Fig. 8). In the delocalized

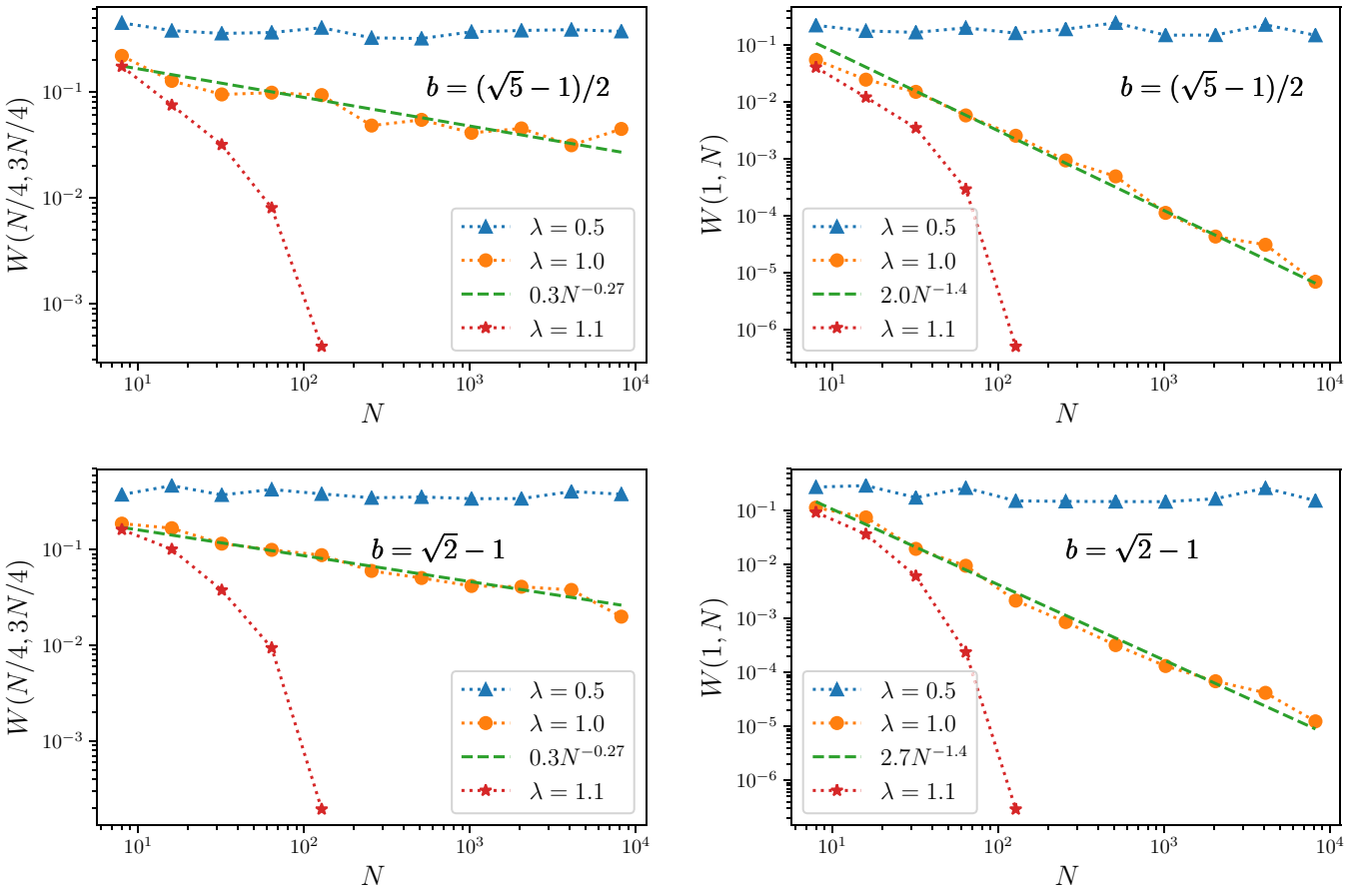

FIG. 7. System-size scaling of $W(N/4,3N/4)$ (left panel) compared with that of $W(1,N)$ (right panel) at all three phases. $W(N/4,3N/4)$ and $W(1,N)$ scale similarly with N away from the critical point: They are independent of N for $\lambda < 1$ and decay exponentially with N for $\lambda > 1$. At the critical point, $\lambda = 1$, $W(N/4,3N/4)$ and $W(1,N)$ show a power-law decay with system size with very different exponents: $W(N/4,3N/4) \sim N^{-0.27\pm0.03}$ whereas $W(1,N) \sim N^{-1.4\pm0.05}$. The system sizes taken here are in powers of 2.

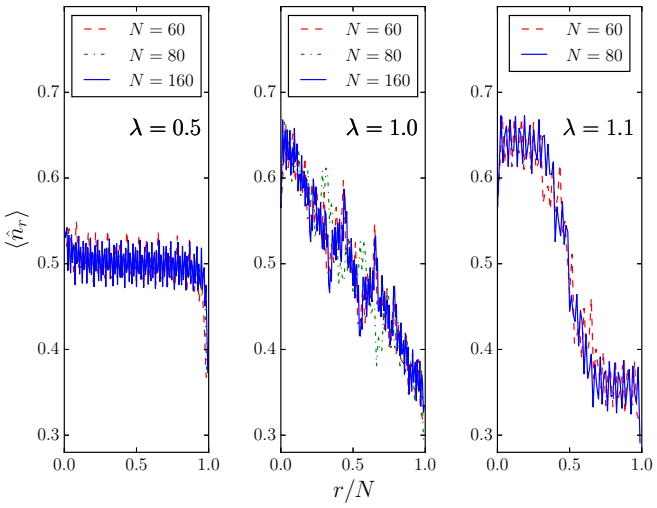

FIG. 8. Open system: NESS particle density profile for the three regimes, delocalized ($\lambda = 0.5 < 1$), critical ($\lambda = 1$), and localized ($\lambda = 1.1 > 1$), for various system sizes. The particle density profile looks distinctly different in the three regimes. Parameters: $\beta = 0.1$, $\mu_1 = 6$, $\mu_2 = -6$, $\gamma = 1$, $t_B = 3$, $b = (\sqrt{5}-1)/2$.

regime, we notice a flat profile, a hallmark of ballistic transport. In the critical regime, we see a continuous (almost linear) curve connecting the boundary densities. Such behavior is typical of diffusive systems. The localized regime shows a steplike profile, and recently this has been reported for other models with localization [68,71]. Hence, this NESS physical quantity, which is potentially measurable with recent cutting-edge experiments [37–40,42], gives a clear real-space signature of localized, critical, and delocalized phases. The energy profile (which is related to local temperature) has a similar behavior.

V. CONCLUSIONS

We have investigated the high-temperature transport properties of the AAH model both in the isolated thermodynamic limit, and in an open system. We have found that the critical point of the AAH model has drastically different transport behavior in the two cases. In the isolated thermodynamic limit, the spread of an initially localized wave packet shows hints of superdiffusive behavior. The superdiffusive scaling exponent is nonuniversal and depends on the choice of the irrational number b. On the other hand, the open system NESS current I scaling with system size N is clearly subdiffusive. There are two subdiffusive exponents. One is $I \sim N^{-1.27\pm0.01}$,

which is seen when system sizes are exactly the denominators of the rational approximants of b, while the other is $I \sim N^{-1.4\pm0.05}$, which is the scaling for generic system sizes. We have shown that the current scaling with system size is entirely controlled by the system-size scaling of eigenfunctions at the boundaries where the baths are attached. Thus, the drastic difference between the isolated and the open system transport properties at the critical point is due to different behaviors of the eigenfunctions at the bulk and at the boundaries.

We would like to point out that looking at the spread of correlations and measuring the current or conductance variation with system size are two different experiments done to characterize transport in many setups. Although not guaranteed, in many cases, the results of one experiment can be inferred from those of the other. We showed that at the critical point of the AAH model, this is not possible.

We have also looked at the NESS particle density profile of an open system connected to two baths at different chemical potentials. We have shown the NESS particle density profile is distinctly different in the delocalized, critical, and localized phases.

After submission of our work, a closely related work appeared [72], where very similar questions were explored using a phenomenological Lindblad quantum master equation approach. On the other hand, in our work, the baths are modeled by microscopic quadratic Hamiltonians having infinite degrees of freedom, and the results are calculated by the fully exact NEGF method. This has no restrictions, for example, it is valid for arbitrary system-bath couplings and fully takes into account non-Markovianity. We find it remarkable that their work reproduces the same results (same scaling of current with system size) as ours. This, in our opinion, is important for the following reason. Because it matches our results, it justifies the use of a phenomenological Lindblad quantum master equation approach, which is often the most practical method for interacting systems [73].

In a followup work, some of the authors (A.P., A.D., and M.K.) investigated open system transport through a generalization of the AAH model where there is a mobility edge [74]. They obtained a high-temperature nonequilibrium phase diagram of that generalized model via current scaling with system size. Detailed investigations of closed system transport and low-temperature transport in a generalized model with a mobility edge is in progress. Note that, while this is easily possible in our approach, the phenomenological Lindblad quantum master equation used in Ref. [72] works only in the infinite-temperature regime and cannot be used to investigate low-temperature physics.

S.S. introduced the rest of the authors to the AAH model and pointed out important references. A.P. did all the calculations and wrote the manuscript. A.D. and M.K. checked all the results, provided crucial physical insights and revised the manuscript.

ACKNOWLEDGMENTS

We would like to thank T. Kottos, H. Spohn, R. Moessner, and A. Kundu for useful discussions. A.D. is thankful for support from the Indo-Israel joint research project No. 6-8/2014(IC) and from the French Ministry of Education through the grant ANR (EDNHS). M.K. gratefully acknowledges support via the Ramanujan Fellowship SB/S2/RJN-114/2016 from the Science and Engineering Research Board (SERB), Department of Science and Technology, Government of India. S.S. acknowledge funding through SERB, Indo-US Science and Technology Forum, Indo-US post-doctoral fellowship.

[1] F. Evers and A. D. Mirlin, Rev. Mod. Phys. **80**, 1355 (2008).
[2] A. Lagendijk, B. van Tiggelen, and D. S. Wiersma, Phys. Today **62**(8), 24 (2009).
[3] A. Aspect and M. Inguscio, Phys. Today **62**(8), 30 (2009).
[4] D. J. Luitz, N. Laflorencie, and F. Alet, Phys. Rev. B **93**, 060201 (2016).
[5] A. C. Potter, R. Vasseur, and S. A. Parameswaran, Phys. Rev. X **5**, 031033 (2015).
[6] K. Agarwal, S. Gopalakrishnan, M. Knap, M. Müller, and E. Demler, Phys. Rev. Lett. **114**, 160401 (2015).
[7] R. Vosk, D. A. Huse, and E. Altman, Phys. Rev. X **5**, 031032 (2015).
[8] S. Aubry and G. André, Ann. Isr. Phys. Soc. **3**, 133 (1980).
[9] P. G. Harper, Proc. Phys. Soc., London, Sect. A **68**, 874 (1955).
[10] D. R. Hofstadter, Phys. Rev. B **14**, 2239 (1976).
[11] R. Ketzmerick, K. Kruse, F. Steinbach, and T. Geisel, Phys. Rev. B **58**, 9881 (1998).
[12] S. Ostlund, R. Pandit, D. Rand, H. J. Schellnhuber, and E. D. Siggia, Phys. Rev. Lett. **50**, 1873 (1983).
[13] A. Avila and S. Jitomirskaya, Ann. Math. **170**, 303 (2009).
[14] Y. Last, Commun. Math. Phys. **164**, 421 (1994).
[15] C. Yang, Y. Wang, P. Wang, G. Xianlong, and S. Chen, Phys. Rev. B **95**, 184201 (2017).
[16] Y. B. Lev, D. M. Kennes, C. Klöckner, D. R. Reichman, and C. Karrasch, Europhys. Lett. **119**, 37003 (2017).
[17] P. Naldesi, E. Ercolessi, and T. Roscilde, SciPost Phys. **1**, 010 (2016).
[18] L. Wang, N. Liu, S. Chen, and Y. Zhang, Phys. Rev. A **95**, 013619 (2017).
[19] D.-L. Deng, S. Ganeshan, X. Li, R. Modak, S. Mukerjee, and J. H. Pixley, Ann. Phys. **529**, 1600399 (2017).
[20] Q.-B. Zeng, S. Chen, and R. Lü, Phys. Rev. B **94**, 125408 (2016).
[21] R. Modak, S. Mukerjee, E. A. Yuzbashyan, and B. S. Shastry, New J. Phys. **18**, 033010 (2016).
[22] X. Li, J. H. Pixley, D.-L. Deng, S. Ganeshan, and S. Das Sarma, Phys. Rev. B **93**, 184204 (2016).
[23] S. Ray, M. Pandey, A. Ghosh, and S. Sinha, New J. Phys. **18**, 013013 (2016).
[24] S. Saha, S. K. Maiti, and S. Karmakar, Physica E **83**, 358 (2016).
[25] V. Mastropietro, Phys. Rev. Lett. **115**, 180401 (2015).
[26] X. Li, S. Ganeshan, J. H. Pixley, and S. Das Sarma, Phys. Rev. Lett. **115**, 186601 (2015).
[27] R. Modak and S. Mukerjee, Phys. Rev. Lett. **115**, 230401 (2015).
[28] S. Ganeshan, J. H. Pixley, and S. Das Sarma, Phys. Rev. Lett. **114**, 146601 (2015).
[29] L. Morales-Molina, E. Doerner, C. Danieli, and S. Flach, Phys. Rev. A **90**, 043630 (2014).

[30] H. Z. Shen, X. X. Yi, and C. H. Oh, J. Phys. B **47**, 085501 (2014).
[31] G. Roósz, U. Divakaran, H. Rieger, and F. Iglói, Phys. Rev. B **90**, 184202 (2014).
[32] A.-M. Guo, X. C. Xie, and Q.-f. Sun, Phys. Rev. B **89**, 075434 (2014).
[33] A. Radosavljević, G. Gligorić, A. Maluckov, and M. Stepić, J. Opt. **16**, 025201 (2014).
[34] S. Iyer, V. Oganesyan, G. Refael, and D. A. Huse, Phys. Rev. B **87**, 134202 (2013).
[35] M. Larcher, T. V. Laptyeva, J. D. Bodyfelt, F. Dalfovo, M. Modugno, and S. Flach, New J. Phys. **14**, 103036 (2012).
[36] M. Tezuka and A. M. García-García, Phys. Rev. A **85**, 031602 (2012).
[37] H. P. Lüschen, P. Bordia, S. Scherg, F. Alet, E. Altman, U. Schneider, and I. Bloch, Phys. Rev. Lett. **119**, 260401 (2017).
[38] H. P. Lüschen, P. Bordia, S. S. Hodgman, M. Schreiber, S. Sarkar, A. J. Daley, M. H. Fischer, E. Altman, I. Bloch, and U. Schneider, Phys. Rev. X **7**, 011034 (2017).
[39] M. Schreiber, S. S. Hodgman, P. Bordia, H. P. Lüschen, M. H. Fischer, R. Vosk, E. Altman, U. Schneider, and I. Bloch, Science **349**, 842 (2015).
[40] C. D. Érrico, M. Moratti, E. Lucioni, L. Tanzi, B. Deissler, M. Inguscio, G. Modugno, M. B. Plenio, and F. Caruso, New J. Phys. **15**, 045007 (2013).
[41] Y. E. Kraus, Y. Lahini, Z. Ringel, M. Verbin, and O. Zilberberg, Phys. Rev. Lett. **109**, 106402 (2012).
[42] Y. Lahini, R. Pugatch, F. Pozzi, M. Sorel, R. Morandotti, N. Davidson, and Y. Silberberg, Phys. Rev. Lett. **103**, 013901 (2009).
[43] G. Roati, C. D. Érrico, L. Fallani, M. Fattori, C. Fort, M. Zaccanti, G. Modugno, M. Modugno, and M. Inguscio, Nature (London) **453**, 895 (2008).
[44] H. Hiramoto and S. Abe, J. Phys. Soc. Jpn. **57**, 230 (1988).
[45] J. Zhong, R. B. Diener, D. A. Steck, W. H. Oskay, M. G. Raizen, E. W. Plummer, Z. Zhang, and Q. Niu, Phys. Rev. Lett. **86**, 2485 (2001).
[46] G. S. Ng and T. Kottos, Phys. Rev. B **75**, 205120 (2007).
[47] R. Ketzmerick, K. Kruse, S. Kraut, and T. Geisel, Phys. Rev. Lett. **79**, 1959 (1997).
[48] B. Everest, I. Lesanovsky, J. P. Garrahan, and E. Levi, Phys. Rev. B **95**, 024310 (2017).
[49] E. Levi, M. Heyl, I. Lesanovsky, and J. P. Garrahan, Phys. Rev. Lett. **116**, 237203 (2016).
[50] M. H. Fischer, M. Maksymenko, and E. Altman, Phys. Rev. Lett. **116**, 160401 (2016).
[51] R. Nandkishore and S. Gopalakrishnan, Ann. Phys. **529**, 1600181 (2017).
[52] S. Banerjee and E. Altman, Phys. Rev. Lett. **116**, 116601 (2016).
[53] S. Johri, R. Nandkishore, and R. N. Bhatt, Phys. Rev. Lett. **114**, 117401 (2015).
[54] D. A. Huse, R. Nandkishore, F. Pietracaprina, V. Ros, and A. Scardicchio, Phys. Rev. B **92**, 014203 (2015).
[55] R. Nandkishore, Phys. Rev. B **92**, 245141 (2015).
[56] R. Nandkishore, S. Gopalakrishnan, and D. A. Huse, Phys. Rev. B **90**, 064203 (2014).
[57] S. Gopalakrishnan and R. Nandkishore, Phys. Rev. B **90**, 224203 (2014).
[58] J. Wang, Y. Zhang, and H. Zhao, Phys. Rev. E **93**, 032144 (2016).
[59] G. Forte, F. Cecconi, and A. Vulpiani, Eur. Phys. J. B **87**, 102 (2014).
[60] M. V. Chubynsky and G. W. Slater, Phys. Rev. Lett. **113**, 098302 (2014).
[61] J. Kim, C. Kim, and B. J. Sung, Phys. Rev. Lett. **110**, 047801 (2013).
[62] B. Wang, J. Kuo, S. C. Bae, and S. Granick, Nat. Mater. **11**, 481 (2012).
[63] B. Wang, S. M. Anthony, S. C. Bae, and S. Granick, Proc. Natl. Acad. Sci. USA **106**, 15160 (2009).
[64] K. H. Andersen, P. Castiglione, A. Mazzino, and A. Vulpiani, Eur. Phys. J. B **18**, 447 (2000).
[65] X. P. Kong and E. G. D. Cohen, Phys. Rev. B **40**, 4838 (1989).
[66] A. Purkayastha, A. Dhar, and M. Kulkarni, Phys. Rev. A **93**, 062114 (2016).
[67] A. Purkayastha, arXiv:1712.01068.
[68] W. De Roeck, A. Dhar, F. Huveneers, and M. Schütz, J. Stat. Phys. **167**, 1143 (2017).
[69] A. Amir, Y. Oreg, and Y. Imry, arXiv:1801.09707.
[70] A. Purkayastha (unpublished).
[71] C. Monthus, J. Stat. Mech.: Theor. Exp. (2017) 043303.
[72] V. K. Varma, C. de Mulatier, and M. Žnidarič, Phys. Rev. E **96**, 032130 (2017).
[73] M. Žnidarič, A. Scardicchio, and V. K. Varma, Phys. Rev. Lett. **117**, 040601 (2016).
[74] A. Purkayastha, A. Dhar, and M. Kulkarni, Phys. Rev. B **96**, 180204 (2017).